Since January 2020 Elsevier has created a COVID-19 resource centre with free information in English and Mandarin on the novel coronavirus COVID-19. The COVID-19 resource centre is hosted on Elsevier Connect, the company's public news and information website.

Computers in Biology and Medicine 142 (2022) 105166

Contents lists available at ScienceDirect

Computers in Biology and Medicine

journal homepage: www.elsevier.com/locate/compbiomed

Detection of COVID-19 severity using blood gas analysis parameters and Harris hawks optimized extreme learning machine

Jiao Hu [a,1], zhengyuan Han [b,1], Ali Asghar Heidari [c,2], Yeqi Shou [b], Hua Ye [d], Liangxing Wang [b], Xiaoying Huang [b], Huiling Chen [a,*], Yanfan Chen [b,**], Peiliang Wu [b,***]

[a] Department of Computer Science and Artificial Intelligence, Wenzhou University, Wenzhou, 325035, China
[b] Department of Pulmonary and Critical Care Medicine, The First Affiliated Hospital of Wenzhou Medical University, Wenzhou, 325000, PR China
[c] School of Surveying and Geospatial Engineering, College of Engineering, University of Tehran, Tehran, Iran
[d] Department of Pulmonary and Critical Care Medicine, Affiliated Yueqing Hospital, Wenzhou Medical University, Yueqing, 325600, China

ARTICLE INFO

Keywords:
Feature selection
Coronavirus disease
Harris hawk optimization
Extreme learning machine
COVID-19
Blood

ABSTRACT

Coronavirus disease-2019 (COVID-19) has made the world more cautious about widespread viruses, and a tragic pandemic that was caused by a novel coronavirus has harmed human beings in recent years. The new coronavirus pneumonia outbreak is spreading rapidly worldwide. We collect arterial blood samples from 51 patients with a COVID-19 diagnosis. Blood gas analysis is performed using a Siemens RAPID Point 500 blood gas analyzer. To accurately determine the factors that play a decisive role in the early recognition and discrimination of COVID-19 severity, a prediction framework that is based on an improved binary Harris hawk optimization (HHO) algorithm in combination with a kernel extreme learning machine is proposed in this paper. This method uses specular reflection learning to improve the original HHO algorithm and is referred to as HHOSRL. The experimental results show that the selected indicators, such as age, partial pressure of oxygen, oxygen saturation, sodium ion concentration, and lactic acid, are essential for the early accurate assessment of COVID-19 severity by the proposed feature selection method. The simulation results show that the established methodology can achieve promising performance. We believe that our proposed model provides an effective strategy for accurate early assessment of COVID-19 and distinguishing disease severity. The codes of HHO will be updated in https://aliasgharheidari.com/HHO.html.

1. Introduction

The International Committee on the Taxonomy of Viruses (ICTV) described a new virus, namely, severe acute respiratory syndrome coronavirus (SARS-CoV-2) [1]. SARS-CoV-2 is believed to be the pathogen that causes viral pneumonia, which has caused a worldwide pandemic [2]. On February 11, 2020, the viral pneumonia that is caused by SARS-CoV-2 was named coronavirus disease 2019 (COVID-19) by the World Health Organization (WHO) [3]. The case fatality ratio (CFR) of COVID-19 is significantly lower than those of severe acute respiratory syndrome (SARS) and Middle East respiratory syndrome (MERS) [4,5]. However, COVID-19's long incubation period of approximately two weeks and the presence of asymptomatic infections increase the risk of COVID-19 virus infection and promote its spread [6]. As of 6:18pm CET, 4 January 2022, according to WHO data[3], COVID-19 has spread globally, with more than 290,959,019 cases of COVID-19 diagnosed in various countries, which have resulted in more than 5,446,753 related deaths (https://www.who.int/).

* Corresponding author.
** Corresponding author.
*** Corresponding author.
E-mail addresses: 194511981394@stu.wzu.edu.cn (J. Hu), hanzy19971128@163.com (Han), as_heidari@ut.ac.ir (A.A. Heidari), 1149044051@qq.com (Y. Shou), 154671045@qq.com (H. Ye), 38805@163.com (L. Wang), zjwzhxy@126.com (X. Huang), chenhuiling.jlu@gmail.com (H. Chen), chenyf2605@163.com (Y. Chen), pl_wu@163.com (P. Wu).

[1] These authors contributed equally to this work.
[2] https://aliasgharheidari.com
[3] World Health Organization. Retrieved January 5, 2022, from https://covid19.who.int/

https://doi.org/10.1016/j.compbiomed.2021.105166
Received 18 September 2021; Received in revised form 20 December 2021; Accepted 20 December 2021
Available online 24 December 2021

The most common clinical manifestation of 2019-nCoV infection includes fever, dry cough, dyspnea, chest pain, myalgia, and fatigue [7]. According to a previous clinical study, 20.7%–31.4% of COVID-19 patients developed a severe form of this disease, such as adult respiratory distress syndrome (ARDS) [8,9]. Furthermore, 4.9%–11.5% of patients with COVID-19 needed advanced life support techniques in the intensive care unit (ICU) [8]. The main characteristics of severe COVID-19 are rapid progression, ARDS, multiple organ dysfunction (MOF), and high fatality rate [10]. According to previous reports, elderly patients with comorbidities are more susceptible to being infected by COVID-19 [11,12]. Moreover, the mortality rate of elderly patients (>65 years old) with comorbidities and ARDS is significantly increased [13].

The rapid progression of COVID-19 places substantial strain on health care systems and hospital critical care resources. Severe COVID-19 patients may experience rapid deterioration if not treated in the ICU timely [14]. Therefore, it is vital to conduct accurate and frequent clinical assessments [8,9,15–17]. However, due to resources being stretched thin and lack of experience and prior knowledge of experts, accurate and frequent assessment is not easy. Effective novel prognostic model systems that can help monitor changes in the condition of COVID-19 patients can guide the effective use of hospital resources. Recently, machine learning methods have been used by many medical workers to help solve medical problems. According to many studies, machine learning (ML) techniques and artificial intelligence (AI) methods have been widely implemented in the diagnosis of COVID-19 [18–21], and many studies have applied swarm intelligence methods to COVID-19 image segmentation [22,23].

Pham et al. [24] trained convolutional neural networks (CNNs) to fine-tune COVID-19 detection in chest slices. Canayaz [25] used deep learning models such as AlexNet, VGG19, GoogleNet, and ResNet to conduct feature extraction and select optimal potential features; two meta-heuristic algorithms, namely, binary particle swarm optimization and binary gray wolf optimization, were used. Al-Falluji [26] et al. utilized X-ray images for deep learning and retrieved essential biomarkers that were related to COVID-19 disease detection. Shaban et al. [27] combined a fuzzy inference engine with deep neural networks (DNNs) to propose a new hybrid diagnostic strategy (HDS) for classifying newly infected individuals to determine whether they are infected. Sun et al. [28] proposed an adaptive feature selection guided deep forest (AFS-DF) approach that is based on chest CT images for COVID-19 classification. Shaban et al. [29] introduced a novel COVID-19 patient detection strategy (CPDS) that is based on hybrid feature selection and enhanced the KNN classifier, which significantly improved the diagnostic accuracy. Dey et al. [30] built various machine learning models for predicting protein–protein interactions (PPIs) between COVID-19 and human proteins and further validated them by biological experiments. Abraham et al. [31] combined multiple CNN-extracted features with a correlation-based feature selection (CFS) technique and a Bayesian classifier for COVID-19 prediction. Liu et al. [32] developed and validated a complete machine learning framework for chest CT images to distinguish COVID-19 from global pneumonia (GP). Tuncer et al. [33] proposed a novel intelligent computer vision method for automatic detection of the COVID-19 virus and conducted 10-fold cross-validation based on the SVM classifier, which showed a classification accuracy of 100.0%. Casiraghi et al. [34] proposed an interpretable machine learning system that provides simple decision criteria for use by clinicians in assessing patient risk. Novitasari et al. [35] used convolutional neural network methods such as feature extraction and support vector machines (SVM) as classification methods to detect whether a patient being examined was healthy, coronavirus-positive, or only had pneumonia.

In this work, we proposed a new machine learning framework, namely, the swarm intelligence augmented kernel extreme learning machine (KELM) [30], for predicting the severity of COVID-19. Notably, for the first time, the binary Harris hawk optimization (HHO)[4], which is improved using specular reflection learning, is used in combination with the KELM classifier for feature selection. The experimental results and simulation results demonstrate the superior performance of the method. The results show that bHHOSRL_KELM performs well in determining which factors play a decisive role in the outcome in COVID-19 diagnosis. The proposed bHHOSRL_KELM was compared with other classifiers, such as fuzzy k-nearest neighbors(FKNN), k-nearest neighbors(KNN), multilayer perceptron (MLP), and support vector machines(SVM), in terms of four classification metrics, namely, classification accuracy, sensitivity, specificity, and Mathews correlation coefficient (MCC). In addition, nine other feature selection methods that are based on swarm intelligence algorithms were used to evaluate the performance of the developed bHHOSRL_KELM based on the fitness values throughout the iterative process. The experimental results show that the developed bHHOSRL_KELM has high predictive performance.

The main contributions of this study are as follows: (1) an efficient diagnostic aid for COVID-19 in blood specimens was developed; (2) a promising hybrid model was proposed, and the potential of KELM was enhanced using an improved HHO method; and (3) the bHHOSRL_KELM feature selection method was used to identify the most critical features effectively.

The remainder of this paper is organized as bellow. The first section describes the current state of research on novel coronaviruses and the application of machine learning methods to novel coronavirus research. The second section presents the dataset that is used in this paper. The third section presents the improved HHO method and its integration with KELM. The fourth section analyze the proposed method and presents the experimental results on COVID-19. The fifth section discusses the proposed method and analyzes the final medical data results.

2. Materials and methods

2.1. Data collection

Our study was approved by the Ethics Committee of the Affiliated Yueqing Hospital of Wenzhou Medical University (Yueqing, China; protocol number 202000002) and complied with the Helsinki declaration. In this single-center retrospective study, our dataset consisted of clinical notes on 51 Chinese COVID-19 patients from a third-level grade-A hospital in eastern China between January 21 and March 10, 2020. The diagnosis was based on the positive detection of SARS-CoV-2 nucleic acid by reverse-transcription polymerase chain reaction (RT–PCR) testing on throat swab samples.

We separated the COVID-19 patient dataset into severe COVID-19, which corresponded to 21 samples, and nonsevere COVID-19, which corresponded to 30 samples. For a diagnosis of severe COVID-19, the following requirements should be satisfied: (1) respiratory rate greater than 30/min (respiratory distress); (2) resting oxygen saturation lower than 93%; and (3) oxygenation index (OI) lower than 300 mmHg. We collected arterial blood samples from all 51 patients with a COVID-19 diagnosis. Blood gas analysis was performed by a SIEMENS RAPID Point 500 blood gas analyzer. The basic clinical information and 22 blood gas analysis parameters (features) are listed in Table 1. All continuity variables are presented as the mean ± standard deviation (SD) and were analyzed with SPSS Statistics 24.0. An independent sample *t*-test was used to analyze the continuous variables (age and blood gas analysis parameters). $p < 0.05$ was considered statistically significant. The statistical analysis results are presented in Table 2.

[4] https://aliasgharheidari.com/HHO.html

Table 1
List of the used features and their abbreviations [36].

	Feature	Abbreviation
F1	Gender	Gender
F2	Age	Age
F3	Hydrogen ion concentration	PH
F4	Partial pressure of carbon dioxide	$PaCO_2$
F5	Partial pressure of oxygen	PaO_2
F6	Oxygen saturation	SaO_2%
F7	Hemoglobin percentage	Hb
F8	Oxyhemoglobin percentage	HbO_2%
F9	Carboxyhaemoglobin percentage	COHb%
F10	Deoxyhemoglobin percentage	DeOxyHb%
F11	Methaemoglobin percentage	MetHb%
F12	Potassium ion concentration	K^+
F13	Sodium ion concentration	Na^+
F14	Chloride ion concentration	Cl^-
F15	Calcium ion concentration	Ca^{2+}
F16	Glucose concentration	GLU
F17	Lactic acid	LAC
F18	Anion gap	AG
F19	Buffer bases	BB
F20	Bases excess	BE
F21	Standard bicarbonate	SB
F22	Actual bicarbonate	AB

Table 2
Comparison of age and blood gas analysis indices between severe COVID-19 and nonsevere COVID-19 [36].

Index	Severe COVID-19 (n = 21)	Nonsevere COVID-19 (n = 30).	p value
Age	61.43 ± 17.64	42.30 ± 11.53	0.00
PH	7.46 ± 0.34	7.43 ± 0.32	0.01
$PaCO_2$	32.10 ± 4.20	37.55 ± 4.51	0.00
PaO_2	65.13 ± 12.45	103.73 ± 27.87	0.00
SaO_2%	92.73 ± 4.20	98.03 ± 1.00	0.00
Hb	13.50 ± 1.98	14.41 ± 2.16	0.13
HbO_2%	91.58 ± 4.28	96.51 ± 0.97	0.00
COHb%	1.01 ± 0.27	1.02 ± 0.26	0.84
DeOxyHb %	6.84 ± 4.29	1.95 ± 0.98	0.00
MetHb %	0.51 ± 0.28	0.52 ± 0.18	0.97
K^+	3.36 ± 0.42	3.32 ± 030	0.68
Na^+	131.00 ± 3.72	136.23 ± 2.74	0.00
Cl^-	103.33 ± 3.37	107.37 ± 3.87	0.00
Ca^{2+}	1.08 ± 0.06	1.12 ± 0.03	0.01
GLU	10.29 ± 3.58	8.16 ± 2.88	0.02
LAC	2.35 ± 1.09	1.70 ± 0.62	0.01
AG	4.86 ± 2.20	4.28 ± 1.41	0.25
BB	−0.24 ± 2.82	0.93 ± 2.48	0.29
BE	−0.86 ± 3.09	0.77 ± 2.79	0.06
SB	24.02 ± 2.55	25.29 ± 2.15	0.06
AB	22.56 ± 3.21	24.58 ± 2.72	0.02

3. Methods

In this study, the improved HHO with specular reflection learning (HHOSRL) mechanism is used as a learning algorithm in the parcel-based feature selection method, and the binary HHOSRL method is used as a feature selection tool to identify the critical features and evaluate the feature subsets using the KELM model. HHO [37] is a new swarm algorithm that was proposed by Heidari et al., in 2019 inside the class of bio-inspired methods [38]. Since its introduction, it has been used in many situations, such as parameter estimation of photovoltaic models. It is a superior method compared to many other algorithms in recent years [39–42], such as the colony predation algorithm (CPA) [43]. HHO has the unique feature that Harris hawks can cooperate in groups to chase prey and adjust the chase pattern according to the dynamics of the situation and the escape pattern of the prey. Since its introduction, HHO has been applied to solve many problems such as parameters identification of photovoltaic cells and modules [44–47], feature selection [48,49], optimizing the machine learning models [21,

50], engineering design problems [47,51,52], web service composition [52], bankruptcy prediction [53], and multi-objective problems [54].

3.1. Exploration phase

Harris hawks perch at random in a specified location and find their prey through 2 strategies, which are expressed mathematically in Eq. (1).

$$X(t+1)=\begin{cases} X_{rand}(t)-r_1|X_{rand}(t)-2r_2X(t)|\ ,\ q\geq 0.5 \\ [X_{rabbit}(t)-X_m(t)]-r_3[lb+r_4(ub-lb)]\ ,\ q<0.5 \end{cases} \tag{1}$$

where $X(t)$ and $X(t+1)$ are the positions of individuals at the current and next iterations, respectively; t is the number of iterations; X_{rand} is the randomly selected individual position; and X_{rabbit} is the prey position, namely, the global optimum of the current evaluation. r_1, r_2, r_3, r_4 and q are random numbers in [0,1], q is used to select the strategy to be used randomly, X_m is the average individual position, $X_k(t)$ is the position of the kth individual in the population and N is the population size.

3.2. Conversion between exploration and exploitation

The HHO algorithm shifts between exploration and various exploitation behaviors based on the prey's escape energy, which is defined as follows:

$$E=2E_0\left(1-\frac{t}{Max\_iter}\right) \tag{2}$$

where E_0 is the initial energy of the prey, which is a random number in [-1,1] that is updated automatically at each iteration; t is the number of iterations; and Max_iter is the maximum number of iterations. The search phase is entered when $|E|\geq 1$, and the exploitation phase is entered when $|E|<1$.

3.3. Exploitation phase

Define r as a random number between [0,1] for choosing the exploitation strategy.

When $0.5\leq|E|<1$ and $r\geq 0.5$, a soft besiege strategy is used to update the position.

$$X(t+1)=\Delta X(t)-E|J\cdot X_{rabbit}(t)-X(t)| \tag{3}$$

where $\nabla X(t)=X_{rabbit}(t)-X(t)$ represents the difference between the prey position and the individual's current position and J is a random number in [0,2].

When $|E|<0.5$ and $r\geq 0.5$, a hard besiege strategy is used to update the position.

$$X(t+1)=X_{rabbit}(t)-E\cdot|\Delta X(t)| \tag{4}$$

When $0.5\leq|E|<1$ and r <0.5, a soft besiege strategy with a progressive rapid dive is used to update the position.

$$X(t+1)=\begin{cases} Y,\ f(Y)<f(X(t)) \\ Z,\ f(Z)<f(X(t)) \end{cases} \tag{5}$$

$$Y=X_{rabbit}(t)-E\cdot|J\cdot X_{rabbit}(t)-X(t)| \tag{6}$$

$$Z=Y+S\times Levy(2) \tag{7}$$

where $f(*)$ is the fitness function; S is a 2-dimensional random vector with elements that are random numbers in [0,1]; and $Levy(*)$ is the mathematical expression for Levy flight.

When $|E|<0.5$ and r <0.5, a soft besiege strategy with a progressive rapid dive is used to update the position.

$$X(t+1)=\begin{cases} Y,\ f(Y)<f(X(t)) \\ Z,\ f(Z)<f(X(t)) \end{cases} \tag{8}$$

$$Y=X_{rabbit}(t)-E\cdot|J\cdot X\_rabbit\ (t)-X_m(t)| \tag{9}$$

$$Z=Y+S\times Levy(2) \tag{10}$$

3.4. Proposed binary HHOSRL

In this paper, we address a binary optimization case, which corresponds to whether a feature is selected or not. In a discrete binary space, a solution is restricted to two numbers (0 and 1). For our case, an upgraded binary HHO is proposed. In this study, we represent a solution as a d-dimensional vector, where d is the number of attributes of the dataset. A value of 1 indicates that the corresponding attribute in the d-dimensional sample is selected, whereas a value of 0 indicates the attribute is not selected. Updating equations such as Eq. (1), Eq. (3), Eq. (4), Eq. (5), and Eq. (8) are useless in dealing with binary optimization tasks since these solutions do not have only two values, namely, "0" and "1". To overcome this problem, the method discretizes the updated hawks' position vector to a binary vector. The updating equation is as follows:

$$X_d(t+1)=\begin{cases} 1\ ,\ S(X_d(t))\geq rand \\ 0\ ,\quad otherwise \end{cases} \tag{11}$$

where $rand$ is a random number in [0,1] and $X_d(t+1)$ is the updated location at the t-th iteration. The expression for $S(x)$ is presented below.

$$S(x)=\frac{1}{1+e^{-10(x-0.5)}} \tag{12}$$

This paper updates the solution using a variation operator based on specular reflection learning (SRL) to further explore more combinations of properties.

$$X^t_{new}(i,j)=(0.5\lambda+0.5)\times\left(U_{max,j}+L_{min,j}\right)-\lambda\cdot X^t(i,j) \tag{13}$$

where $X^t_{new}(i,j)$ is the binary value of the $j-$ th dimension of the i-th individual in the t-th iteration after mutation and λ is a variable that controls the range of the new position after specular reflection, which is calculated via Eq. (14).

$$\lambda=\begin{cases} 1+\varphi R_0,\ if\ k_1>k_2 \\ 1-\varphi R_0,\ otherwise \end{cases} \tag{14}$$

where k_1 and k_2 are two random numbers that are uniformly distributed between 0 and 1 and R_0 is the neighborhood radius, which is also called the elasticity factor. From Eq. (14), if $k_1>k_2$, X^t_{new} will appear in the right neighborhood of X^t; otherwise, X^t_{new} will appear in the left neighborhood of X^t. Therefore, it is reasonable to set R_0 to [0,1] to balance the search space of the left and right neighbors. Additionally, φ is also set to [0,1], namely, all possible values within a radius R_0 of the neighborhood are obtained.

Algorithm 1. Procedure of HHOSRL

Initialize a set of binary hawks (X_i, i=1…N) and the probability of mutation J_r;
While t < *Max_iter*
Calculate the fitness with the selected feature subset for each hawk;
Set the individual with the lowest fitness to X_{rabbit};
Update each individual's escape ability E and jump strength J;
If$|E| \geq 1$
Update the position vector X by $Eq.(1)$;
Else if $|E| < 1$
If $r \geq 0.5$ and$|E| \geq 0.5$
Update the position vector X by $Eq.(2)$;
End
If $r \geq 0.5$ and$|E| < 0.5$
Update the position vector X by $Eq.(3)$;
End
If $r < 0.5$ and$|E| \geq 0.5$
Update the position vector X by $Eq.(4)$;
End
If $r < 0.5$ and$|E| < 0.5$
Update the position vector X by $Eq.(5)$;
End
End
Binarize X via $Eq.(12)$;
Generate a random value η;
If $\eta < J_r$
Calculate U_{max} and L_{min};
Calculate λ by $Eq.(15)$;
Generate a new solution X_{new} using the mutation operator (mirror reflection learning);
END
Binarize X_{new} via $Eq.(12)$;
Update X by X_{new} greedily;
t = t + 1;
Update the optimal position X_{rabbit};
End while
End

4. Classification based on KELM

4.1. KELM

The ELM is a special kind of single-implicit feedforward neural network with three separate layers: input, hidden, and output. For a dataset of N training samples $(x_j, t_j) \in R_n \times R_m$, when the number of implicit layer nodes of the ELM is L and the excitation function is ϑ:

$$f(x_i) = \sum_{i=1}^{L} \beta_i \vartheta(\omega_i x_j + b_i) = t_j,\ j = 1, \ldots, N \tag{15}$$

where the vector of weights between the $i-th$ hidden layer node and the output layer node is β_i. ELM differs completely from traditional iterative learning algorithms in that it randomly selects the input weights ω and bias b of the implicit layer nodes before analytically calculating the least-square solution of the output weights β. Reducing the training error rate and optimizing the generalization capabilities are the goals of these calculations.

Eq. (15) is expressed in a compact form according to ELM theory:

$$H\beta = T \tag{16}$$

After the excitation function and the number of implicit layer nodes are established, the following 3 steps are conducted to train the ELM on a training dataset.

Step 1. Randomly generate input weights ω_i and b_i, $1 \leq i \leq N$;

Step 2. Calculate the output matrix of the hidden layer H;

Step 3. Calculate the output weight matrix $\beta = H^+ T$;

where H^+ is the Moore-Penrose generalized inverse of the implicit layer output matrix H. When HH^T is nonsingular, $H^+ = H^T(HH^T)^{-1}$.

To eliminate errors in the results of the "sick matrix," according to the strategy of ridge regression, a regularization factor η is introduced, and the least-squares solution of the output weights of the network is

$$\beta = H^T\left(HH^T + \eta I\right)^{-1} T \tag{17}$$

Therefore, the corresponding ELM output function is

$$y(x) = h(x)\beta \tag{18}$$

If the feature mapping function h(x) is not known, a new kernel-based ELM (KELM) method can be formed by introducing a kernel function into the ELM. In the KELM method, we need to define the kernel

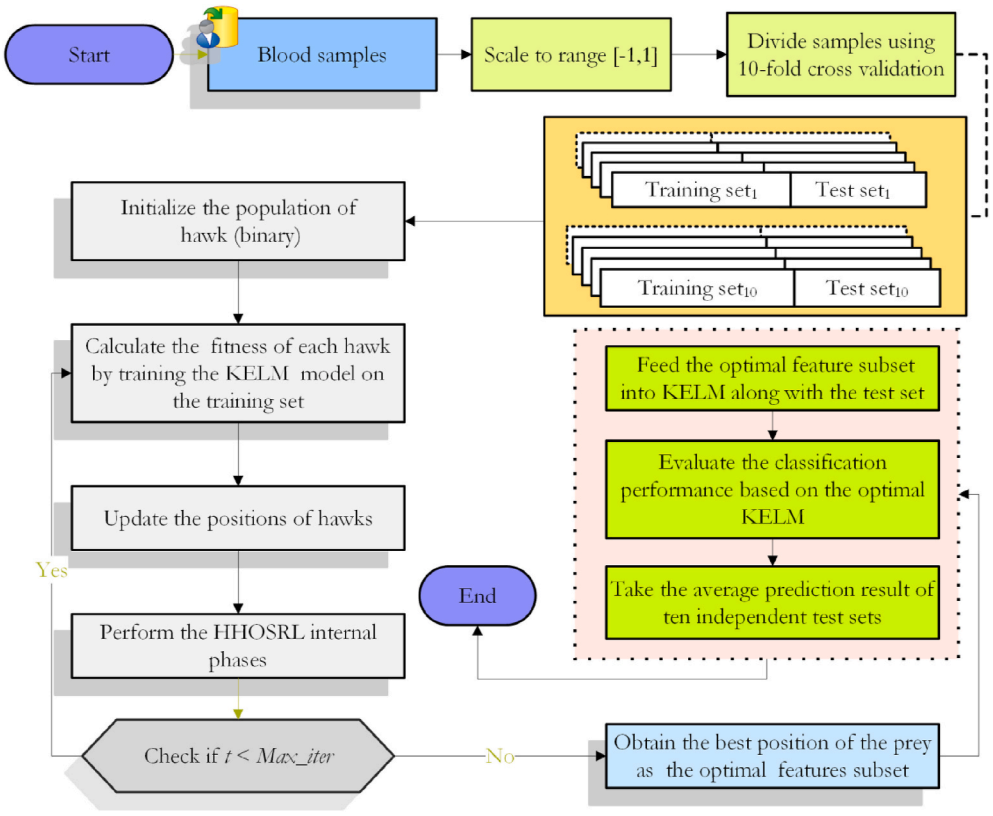

Fig. 1. Flowchart of the HHOSRL-KELM

matrix $QELM = HH^T$, which has the following elements:

$$Q_{ELM}(i,j) = h(x_i) \cdot h(x_j) = K(x_i, x_j) \tag{19}$$

Then, using Eq. (18), the network output can be expressed as follows:

$$y(x) = \begin{bmatrix} K(x, x_1) \\ \vdots \\ K(x, x_N) \end{bmatrix} (\eta I + Q_{ELM})^{-1} T \tag{20}$$

In Eq. (20), the radial basis kernel function is selected as the kernel function $K(x_i, x_j)$:

$$K(x_i, x_j) = \exp\left(-\frac{||x_i - x_j||^2}{\gamma^2} \right) \tag{21}$$

where γ is the nuclear parameter of the RBF kernel function.

The two key parameters have been shown to have a large impact on the performance of KELM on many problems, such as second major prediction [55], medical diagnosis [56–61], financial stress prediction [62,63], and recognition of foreign fibers in cotton [64].

4.2. Proposed HHOSRL-KELM

To find more representative attributes in the dataset to help us make a medical diagnosis, this paper uses HHOSRL-KELM as a feature selection method to choose the optimal feature subset. First, we use HHOSRL as the optimization algorithm to find the optimal subset, and after finding the optimal features, we use KELM as the classifier for the classification task. Fig. 1 shows a HHOSRL-KELM flowchart. It illustrates the process of finding key factors for a new coronary pneumonia blood sample. The main steps of the HHOSRL-KEML method are described below.

Step 1. Initialize the parameters of the HHOSRL method, such as population size, search space boundary, variance probability, maximum number of iterations, and initial escape energy.

Step 2. Randomly initialize the binary population of Harris hawks.

Step 3. Use the agent's binary value in each dimension to represent the subset selection of the dataset (1 indicates that the feature is selected, and 0 indicates that it is not selected).

Step 4. Calculate the fitness value of the selected feature subset for each hawk as follows:

$$F(x) = \alpha \cdot error + \beta \cdot \frac{|R|}{|D|} \tag{22}$$

where *error* is the classification error rate of KELM, $|D|$ is the number of features in the data sample, $|R|$ represents the number of features in the selected feature subset, α and β are two weights that reflect the importance of the classification error rate and the length of the selected features, respectively In this paper, we set $\alpha = 0.99$ and $\beta = 0.01$, which are values that are commonly used in many works [48,49].

Step 5. Update the population of agents according to the HHOSRL algorithm.

Step 6. Select the individual with the smallest fitness value as the optimal solution.

Table 3
Parameter settings for the five methods.

Method	Parameter values
bHHOSRL_FKNN	$K = 1, m = 2$
bHHOSRL_SVM	$C = 850, \gamma = 0.17$
bHHOSRL_KNN	$K = 1$
bHHOSRL_MLP	$C = 88, \gamma = 1024$
bHHOSRL_KELM	$M = 1$

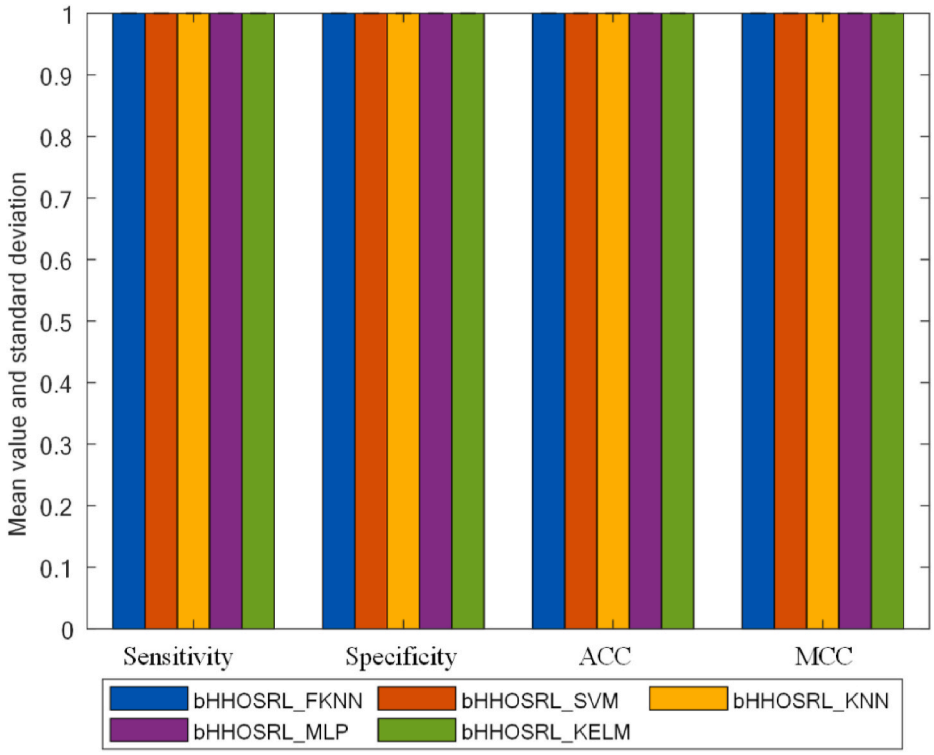

Fig. 2. Comparison of HHOSRL on five well-known classifiers.

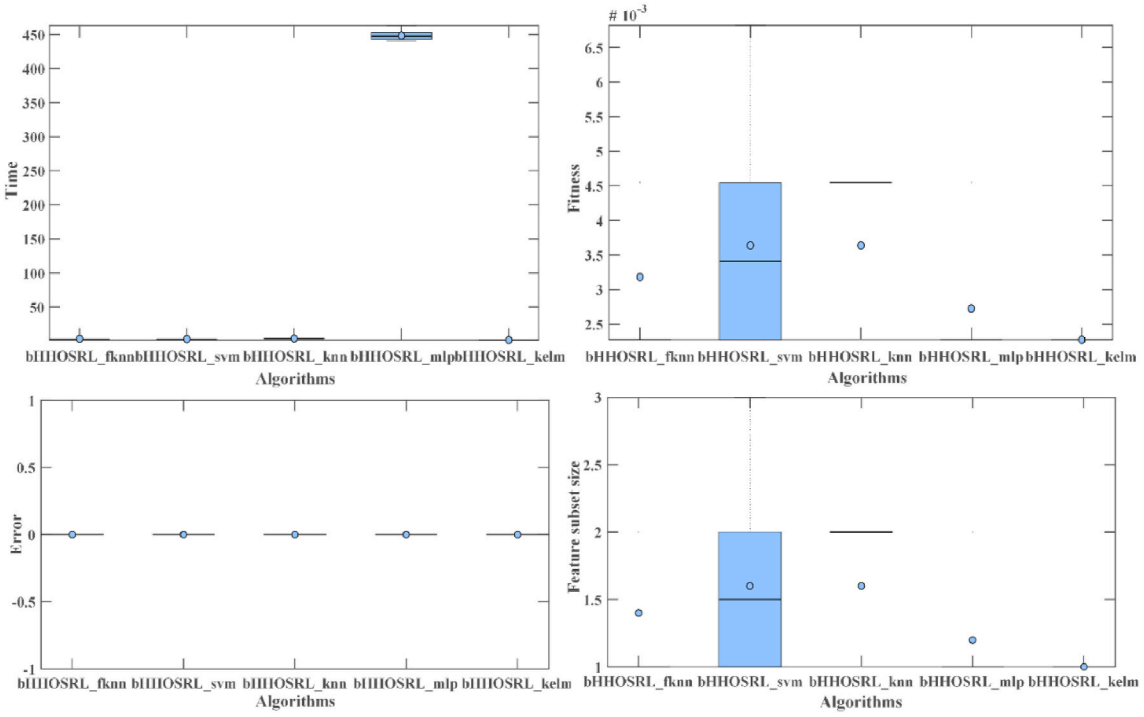

Fig. 3. Boxplot of the classification performances of the four methods in terms of time, fitness, error, and size.

Step 7. Determine whether the termination condition has been reached, namely, whether the maximum number of iterations has been reached. If yes, proceed to the next step; otherwise, repeat Step 3 until the termination condition is met.

Step 8. Return the final optimal solution as the selected feature subset.

Step 9. Use the final feature subset as the input parameter of KELM to obtain the final classification result.

Step 10. Using the classification results that were obtained in Step 9, calculate the classification error accuracy, number of selected feature subsets, sensitivity, specificity, and other evaluation criteria.

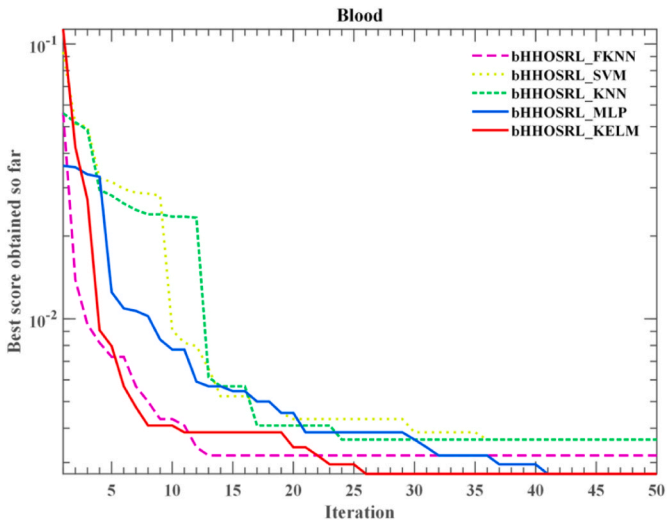

Fig. 4. Convergence evolution trends of the five methods.

5. Experiments and analysis

5.1. Experimental setup

To verify the effectiveness of the proposed HHOSRL-KELM method, the traditional BHHO, bGWO, bMFO, bWOA, and BPSO were used for comparison. bHHO is a binary HHO algorithm that is obtained by discretizing the original HHO algorithm with the sigmoid method. bGWO, bMFO, bWOA, and BPSO are feature selection algorithms that were proposed by various scholars and perform well on the UCI dataset. Additionally, to further evaluate the performance of the HHOSRL, experiments were also done on a practical dataset to evaluate the performance of the HHOSRL in combination with various classifiers. The blood samples were normalized to the range of [−1,1] before developing the classification model. For comparison purposes, all implementations were performed using the same simulation parameters, as per rules for fair comparisions in machine learning [65]. The max_iter and popsize were set to 50 and 20, respectively. Other parameters in WOA, MFO, and GWO were set to those that were used in the original manuscripts [66–68]. Classification performance was evaluated using 10-fold cross-validation (CV) analysis to obtain an objective result. Additionaly, to evaluate the performance of HHOSRL-KELM, we considered five commonly used evaluation criteria: classification accuracy (ACC), specificity, sensitivity, number of selected feature subsets, and MCC [69].

5.2. Performance metrics

We utilized four mutual rules based on the confusion matrix to validate the efficacy of the classifier. Full definitions of these metrics are provided in Refs. [70,71]. Here, we present their formulas to avoid discussions that are outside the scope of this study:

$$Accuracy = \frac{TP + TN}{TP + TN + FP + FN} \tag{23}$$

$$Specificity = \frac{TN}{FP + TN} \tag{24}$$

$$Sensitivity = \frac{TP}{TP + FN} \tag{25}$$

where all variables are as defined in Ref. [71]. In addition, the MCC was used to carefully evaluate the classifier's performance because it provides an objective predictive valuation [72].

$$MCC = \frac{TP \times TN - FP \times FN}{\sqrt{(TP + FP) \times (TP + FN) \times (TN + FP) \times (TN + FN)}} \tag{26}$$

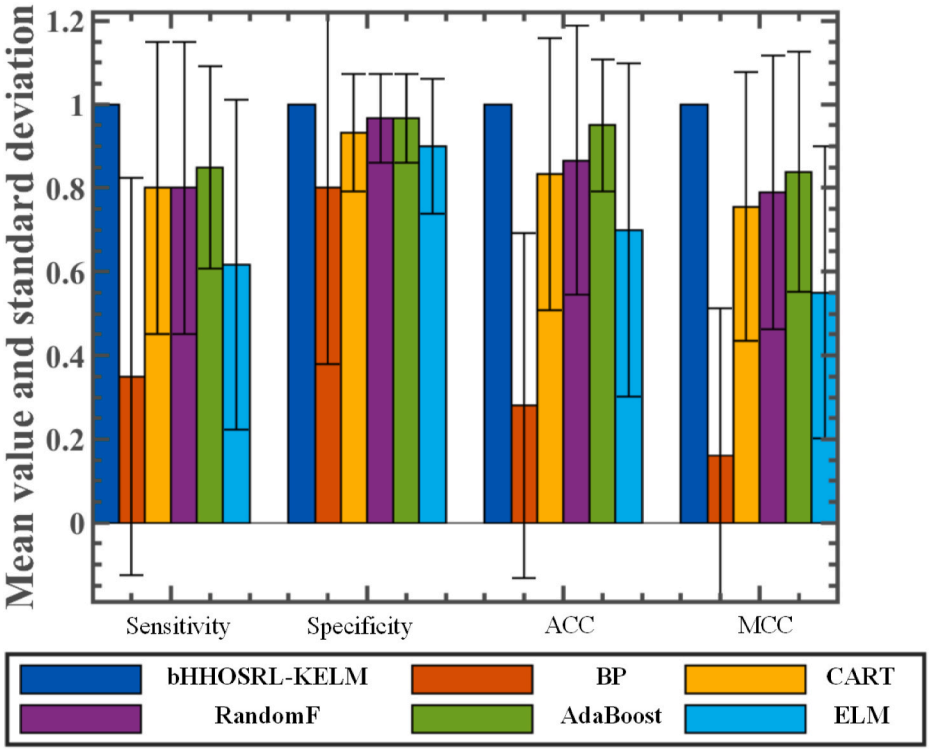

Fig. 5. Comparison of bHHOSRL_KELM with well-known classifiers.

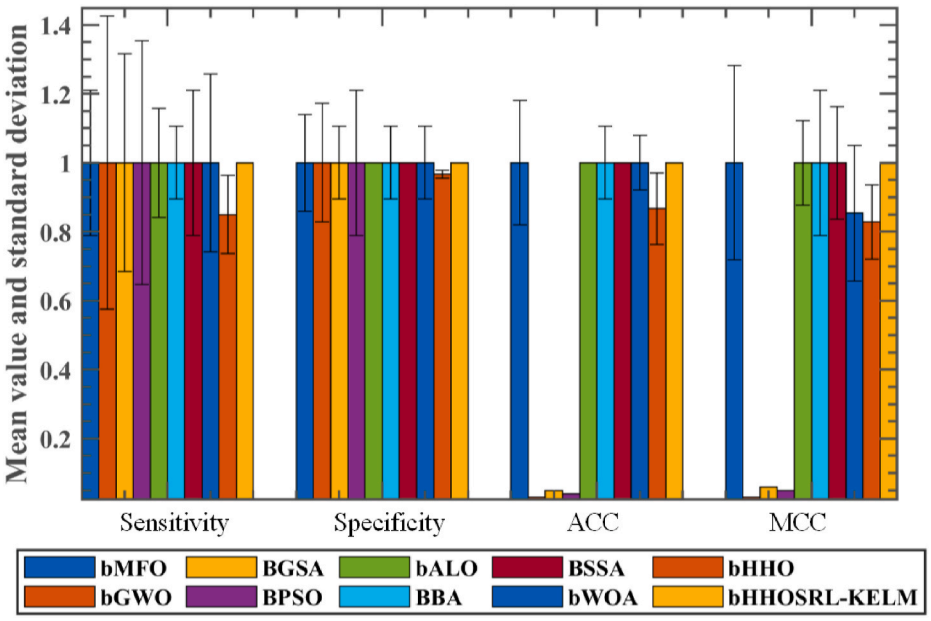

Fig. 6. Comparison results of 10 algorithms on four classification criteria.

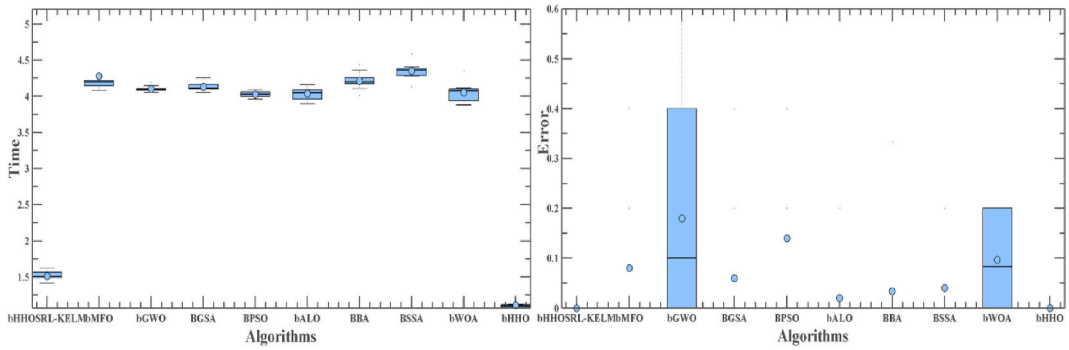

Fig. 7. Boxplot of the performances of the ten methods in terms of error and time consumption.

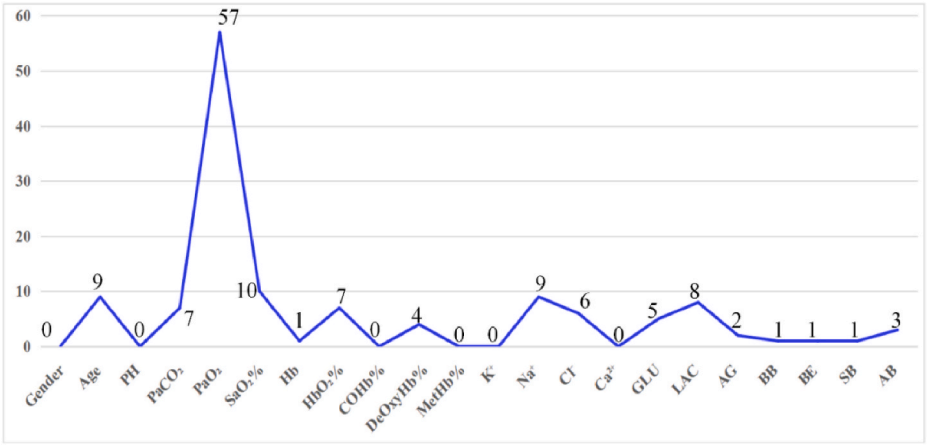

Fig. 8. Selected features by the bHHOSRL_KELM during the 10-fold CV procedure.

5.3. Analysis of the experimental results

It is well known that classification methods play an important role in the performance of wrapped feature selection approches [20,73–78]. Therefore, to evaluate the performance of the proposed HHOSRL method, it was combined with five classification methods, namely, SVM, KNN, FKNN, MLP, and KELM, and applied to the feature selection of blood samples. To evaluate the reliability of the results, we analyzed these five feature selection methods on blood data in terms of four aspects: MCC, ACC, sensitivity, and specificity. The parameter settings of

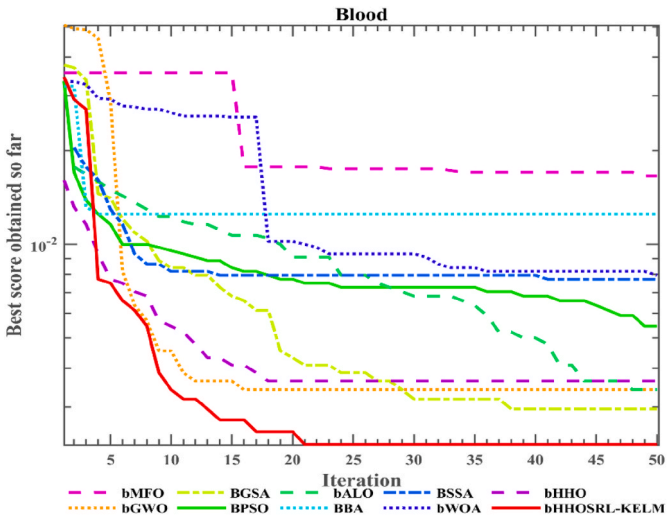

Fig. 9. Convergence evolution trends of ten methods.

these five classification methods are presented in Table 3.

Fig. 2 shows error bar graphs for the five methods on these four criteria. The error line is the magnitude of the mean confidence space, which represents the standard error and is used to visualize the magnitude of the standard deviation. It can be easily observed from the graph that all five classification methods achieve a result of 1 on this criterion and that the error results are all 0. This is sufficient to prove that HHOSRL has a strong learning performance and can accurately find the globally optimal solution. It also shows that HHOSRL has strong stability.

In addition to these four evaluation criteria, to compare the advantages and disadvantages of HHOSRL using these five classifiers, the five feature selection algorithms were also analyzed in terms of time consumption, fitness value, size of the selected feature subset and classification error rate.

Fig. 3 is a box plot, which is used to view possible outlier data conditions. The blue points in the graph are called error points. The upper and lower middle-box lines represent the upper and lower quartiles with a specified resistance. A horizontal line in the middle represents the median, which reflects the distribution of the experimental results. As shown in the graph, all the time consumptions are relatively small except for that of bHHOSRL_MLP. All the algorithms have small fitness values except for bHHOSRL_SVM, which has a large fitness value and is not concentrated. All the algorithms have classification error rates of 0. Finally, in terms of the size of the feature subset, bHHOSRL_SVM does not perform very well, and the values for bHHOSRL_FKNN and bHHOSRL_KNN are relatively large. The most stable subset size is obtained by bHHOSRL_KELM. Therefore, we finally selected bHHOSRL_KELM as the wrapper method. The convergence plot of the average fitness value from 50 iterations in Fig. 4 shows that bHHOSRL_KELM has the fastest convergence speed and the smallest convergence value.

After determining the classification method, we used bHHOSRL_KELM as the final feature selection method and compared it with eight feature selection methods that were proposed by other scholars and with the feature selection method after discretizing the original HHO. The performance of bHHOSRL_KELM was evaluated in terms of MCC, ACC, sensitivity, and specificity, which are the four commonly agreed upon classification accuracy metrics, and in terms of time consumption, classification error rate, and convergence of the fitness values of the algorithmTo evaluate the impacts of the feature selection part and the efficiency of the developed HHO-based core in the bHHOSRL_KELM technique, we compared it with the method without feature selection. The method was compared with a set of well-regarded classifiers, such as classification decision tree (CART), BP, extreme learning machine (ELM), the ensemble methods including (AdaBoostM1) and RF. We utilized the BP algorithm, CART, RandomF, and AdaBoostM1 in the self-built classifiers from the MATLAB toolbox. The ELM method is available at http://www.ntu.edu.sg/eee/icis/cv/egbhuang.htm. We present the results of the six classifiers in Fig. 5. As shown in Fig. 5, the proposed bHHOSRL_KELM method with feature selection outperforms the basic classifier without the HHO-based strategy. In addition, the bHHOSRL_KELM technique is the best performing model on the blood dataset in terms of four performance metrics.

Fig. 5 shows that among the six classification methods, bHHOSRL_KELM performs the best, and AdaBoost ranks second. Pure ELM does not perform best on the blood dataset. This shows that the HHOSRL algorithm in bHHOSRL_KELM can effectively compensate for the disadvantages of the simple classifier in classification to achieve better results.

To further evaluate the effectiveness of the developed bHHOSRL_KELM on the blood dataset, bHHOSRL_KELM was compared with common algorithms, namely, bGWO, bMFO, BGSA, bALO, BPSO, BSSA, bWOA, and BBA.

Fig. 6 compares these ten algorithms on the four evaluation criteria. As shown in the figure, bGWO, BGSA, and BPSO perform poorly in terms of ACC and MCC. Four algorithms, namely, bMFO, bALO, BBA, and BSSA, reach the maximum value of 1 in most cases on these four criteria. However, according to the error line, these four algorithms have many errors. bHHO does not reach the optimum on any of the four criteria. Finally, the error bar graph of bHHOSRL_KELM shows that the overall accuracy is the highest and the error is the smallest; hence, bHHOSRL_KELM has the best results on these ten feature selection methods.

To fully analyze the performance of the bHHOSRL_KELM algorithm, we also compared the algorithm in terms of classification error rate and time consumption. Fig. 7 shows that the classification error rates are larger for bMFO, BBA, BSSA, and bWOA. There are anomalous data points in bGWO, BPSO, bALO, and bHHO in the tenfold cross-validation. This indicates that these algorithms are not very stable. In contrast, bHHOSRL_KELM always attains a value of 0 for both the overall distribution and the anomalies. Therefore, bHHOSRL_KELM has both higher stability and higher classification accuracy. An analysis of the algorithm's classification performance must also consider the time consumption. bHHO is the least time-consuming, and bHHOSRL_KELM is the second most time-consuming. Overall, the classification performance of bHHOSRL_KELM is the best.

Finally, the results of the feature selection were analyzed. To determine whether the subset of features that were selected by bHHOSRL_KELM are substantially helpful for medical diagnosis, tenfold cross-validation of the classification results was performed in this paper. The number of times that each feature was selected in each experiment was counted. The results are presented in the form of a line graph in Fig. 8. According to the graph, age, PaO_2, SaO_2%, Na^+, and LAC were selected the most times. PaO_2 was selected 57 times; hence, PaO_2 was the most important factor that influenced the determination of whether a patient was infected with the new coronavirus. The next most important attribute was SaO_2%, which was selected ten times. This also suggests that SaO_2% plays a role in the final outcome diagnosis. Age and Na^+ were checked nine times, thereby indicating that age and Na^+ can facilitate final diagnosis. Finally, LAC was selected eight times. This shows that LAC is also a factor that cannot be ignored in diagnosis. Fig. 9 shows the convergence graphs of these ten algorithms, which were used to analyze the convergence accuracy and convergence speed of bHHOSRL_KELM. As shown in the graph, in terms of both convergence speed and convergence accuracy, bHHOSRL_KELM performs the best, and BGSA and bGWO perform the next best.

6. Discussion

In this study, a KELM-based feature selection method was used to screen a dataset of COVID-19 patients. Then, we screened several key

features, including age, PaO_2, SaO_2%, Na^+, and LAC. Subsequently, the bHHOSRL_KELM model was constructed to accurately assess the severity of COVID-19 and monitor its early progression. Therefore, we believe that the use of the bHHOSRL_KELM model can make a more accurate clinical decision-making. Due to its great optimization capability, the proposed HHOSRL algorithm can also be applied to solve other problems, such as problems in video deblurring [79], microgrid planning [80], information retrieval services [81–83], image dehazing [84], image fusion [85], kayak cycle phase segmentation [86], human motion capture [87], fault detection [88], virus detection [89], video coding optimization [90], outlier detection [91], location-based services [92,93], image retrieval [94], multivariate time series analysis [95] and multi-objective problems [96].

Previous studies have shown that age is an important independent indicator for predicting the prognosis of SARS and MERS [97,98]. In the study, Smits et al. found that elderly macaques that were vaccinated with SARS coronavirus showed stronger host innate responses than younger macaques, which may be related to the increased differential expression of inflammation-related genes and reduced expression of type I interferon β [99]. Similar to SARS and MERS, Zhou et al. found that the mortality rate of COVID-19 patients increases with age [100]. Through multivariate analysis, other studies show that in COVID-19 patients, advanced age is an independent risk factor for pneumonia. Moreover, patients with ARDS are older than those without ARDS [101]. Furthermore, another study found that elderly patients have a higher probability of developing sepsis, which may be related to age-dependent defects in lymphocyte function and excessive production of type 2 cytokines [102]. In summary, age is an essential predictor of the prognosis of COVID-19 patients.

SaO2 is the percentage of the volume of HbO2 that is bound by oxygen in the blood relative to the total volume of bound hemoglobin. PO_2 is the tension that is produced by oxygen that is physically dissolved in the blood [103]. Xie et al. found that hypoxemia in COVID-19 patients is associated with mortality [104]. Hypoxia has been reported to increase angiotensin I-converting enzyme 2 (ACE-2) expression at the transcription and protein levels in human cells [105,106]. According to reports, ACE2 is the target receptor that SARS-CoV-2 enters. Moreover, the binding affinity of the SARS-CoV-2 spike protein to the ACE2 receptor is 10–20 times higher than that of SARS-CoV [107]. The high affinity of ACE2 and the SARS-CoV-2 spike protein may explain some complications of COVID-19 patients, including acute renal failure, cardiovascular and cerebrovascular diseases. Diffuse endotheliitis and microthrombi formation may be an important pathogenesis mechanism for COVID-19 [108,109]. Therefore, hypoxia may aggravate the severity of COVID-19 by upregulating the target receptor for virus entry. Additionally, in the presence of microthrombi, hypoxemia will cause a higher degree of hypoxia and damage to peripheral tissues [110]. Based on the above considerations, SaO_2 and PO_2 may be powerful predictors of the severity of COVID-19.

Sodium ions (Na^+), which are the most abundant cations in the extracellular fluid, are essential for maintaining the volume of the extracellular fluid, regulating the acid-base balance, maintaining the normal osmotic pressure and cell physiological functions, and participating in the normal physiological activities of the nerve and muscle system [111]. In early COVID-19 studies, the sodium ion concentration in the severe COVID-19 group was significantly lower than the concentration in the nonsevere COVID-19 group [112,113]. In a study that was based on 59 COVID-19 patients, Huang and colleagues found that the sodium ion concentration in ICU care groups was lower than that in no ICU care groups [11]. Our study also found that the average sodium ion concentration in severe patients, namely, 131.00 mmol/L, was lower than that in nonsevere patients, namely, 136.23 mmol/L ($p < 0.01$). Therefore, serum sodium ion concentration may also be an essential indicator for predicting severe COVID-19.

Lactic acid (LAC) is an intermediate product of sugar metabolism. Increased glucose metabolism or decreased pyruvate metabolism will increase the production of lactic acid. In sepsis, the inflammation response is associated with increased glycolysis and impaired pyruvate dehydrogenase. At this time, the metabolism of pyruvate is limited; hence, the concentration of pyruvate increases. To maintain a normal ratio of pyruvate to lactic acid, the lactic acid concentration will increase [114]. Therefore, LAC can be used as an indicator of the severity of inflammation in patients. A study of 1461 patients showed that the mortality rate of COVID-19 patients with high lactate levels was approximately twice that of patients with low lactate levels [115]. Although cell breakdown under conditions of critical illness may also play a role, the increase in lactic acid in COVID-19 patients may be caused by increased glycolytic activity in multiple cell types [116]. Moreover, an inflammatory factor, namely, interleukin 6, which induces lactic acid production, is present at high concentration in patients with COVID-19. In conclusion, LAC can be used as a predictor of the severity of COVID-19 disease.

Up to now, few studies have utilized blood gas analysis parameters or clinical information to distinguish the severity of the COVID-19. To the best of our knowledge, this is the first study to predict the prognosis of COVID-19 using machine learning methods based on age, PaO_2, SaO_2%, Na^+, and LAC. However, this study has several limitations. First, our data originated from a single third-level grade-A hospital in the east of China, and the sample size is not large enough. This limits the accuracy of the prediction. We will expand the sample size in future studies. Second, multicenter, large independent/external datasets and prospective studies need to be conducted to validate the results.

7. Conclusions and future work

This article begins with a description of the current status of COVID-19 and the tremendous strain it places on health care systems and hospital critical care resources. It also describes in detail the sources of the data that are used in this paper. Later, the methodology that is proposed is described in detail. First, the basic HHO algorithm is described. Then, the improvement strategy that is proposed in this paper is presented. Finally, its fusion with the KELM classifier is used to filter out essential features from a blood sample dataset. To evaluate the performance of the proposed method, HHOSRL is fused with various classifiers, and it is demonstrated that HHOSRL produces satisfactory results using many of these classifiers. An accuracy of almost 100.00% is achieved. Then, it is determined that fusion with the KELM classifier enables HHOSRL to perform best on blood samples. After determining the best classifier, the proposed method is compared with various swarm intelligence feature selection methods. It is found that the proposed bHHOSRL_KELM achieves almost 100.00% specificity, accuracy, sensitivity, and MCC. The time consumption of bHHOSRL_KELM is much less than those of other feature selection methods. Finally, the five features that were selected most frequently in the experiment were selected by this method. Moreover, the roles of these five features in medical diagnosis are discussed.

For future work, several issues merit further consideration. Additional influencing factors and coefficients can be included in the investigation, and in our paper, only the available data are presented. Moreover, parallel computing can be used to decrease the computational load during various applications. Additionally, more data samples can be collected to construct a more efficient and reliable framework. Finally, bHHOSRL_KELM can be used for the diagnosis of other diseases, and the algorithm's application scope can be expanded, e.g., to clustering and CT image segmentation.

Declaration of competing interest

The authors declare that there is no conflict of interests regarding the publication of article.

Acknowledgments

This work was supported in part by the Natural Science Foundation of Zhejiang Province (LZ22F020005), National Natural Science Foundation of China (62076185 and U1809209), Beijing Natural Science Foundation (L182015). We acknowledge the comments of the reviewers.

References

[1] Coronaviridae Study Group of the International Committee on Taxonomy of Viruses. "The species Severe acute respiratory syndrome-related coronavirus: classifying 2019-nCoV and naming it SARS-CoV-2." Nat. Microbiol., vol. 5,4 (2020): 536-544. doi:10.1038/s41564-020-0695-z.

[2] Z. Zhang, F. Cui, C. Cao, Q. Wang, Q. Zou, Single-cell RNA analysis reveals the potential risk of organ-specific cell types vulnerable to SARS-CoV-2 infections, Comput. Biol. Med. 105092 (2021), https://doi.org/10.1016/j.compbiomed.2021.105092.

[3] C.C. Lai, T.P. Shih, W.C. Ko, H.J. Tang, P.R. Hsueh, Severe acute respiratory syndrome coronavirus 2 (SARS-CoV-2) and coronavirus disease-2019 (COVID-19): the epidemic and the challenges, Int. J. Antimicrob. Agents 55 (2020) 105924.

[4] A.A. Rabaan, S.H. Al-Ahmed, S. Haque, R. Sah, R. Tiwari, Y.S. Malik, K. Dhama, M.I. Yatoo, D.K. Bonilla-Aldana, A.J. Rodriguez-Morales, SARS-CoV-2, SARS-CoV, and MERS-COV: A comparative overview, Infezioni Med. Le 28 (2020) 174–184.

[5] N. Petrosillo, G. Viceconte, O. Ergonul, G. Ippolito, E. Petersen, COVID-19, SARS and MERS: are they closely related? Clin. Microbiol. Infect. 26 (2020) 729–734.

[6] Z. Wu, J.M. McGoogan, Characteristics of and important lessons from the coronavirus disease 2019 (COVID-19) outbreak in China: summary of a report of 72 314 cases from the Chinese center for disease control and prevention, JAMA 323 (2020) 1239–1242.

[7] H. Harapan, N. Itoh, A. Yufika, W. Winardi, S. Keam, H. Te, D. Megawati, Z. Hayati, A.L. Wagner, M. Mudatsir, Coronavirus disease 2019 (COVID-19): a literature review, J Infect Public Health 13 (2020) 667–673.

[8] CDC COVID-19 Response Team, Severe Outcomes Among Patients with Coronavirus Disease 2019 (COVID-19) - United States, February 12-March 16, 2020, MMWR. Morbidity and mortality weekly report 69 (12) (2020) 343–346, https://doi.org/10.15585/mmwr.mm6912e2.

[9] Q. Zhao, M. Meng, R. Kumar, Y. Wu, J. Huang, Y. Deng, L. Yang, Lymphopenia is associated with severe coronavirus disease 2019 (COVID-19) infections: a systemic review and meta-analysis, Int. J. Infect. Dis. 96 (2020) 131–135.

[10] N. Chen, M. Zhou, X. Dong, J. Qu, F. Gong, Y. Han, Y. Qiu, J. Wang, Y. Liu, Y. Wei, J. Xia, T. Yu, X. Zhang, L. Zhang, Epidemiological and clinical characteristics of 99 cases of 2019 novel coronavirus pneumonia in Wuhan, China: a descriptive study, Lancet 395 (2020) 507–513.

[11] C. Huang, Y. Wang, X. Li, L. Ren, J. Zhao, Y. Hu, L. Zhang, G. Fan, J. Xu, X. Gu, Z. Cheng, T. Yu, J. Xia, Y. Wei, W. Wu, X. Xie, W. Yin, H. Li, M. Liu, Y. Xiao, H. Gao, L. Guo, J. Xie, G. Wang, R. Jiang, Z. Gao, Q. Jin, J. Wang, B. Cao, Clinical features of patients infected with 2019 novel coronavirus in Wuhan, China, Lancet 395 (2020) 497–506.

[12] L. Roncon, M. Zuin, G. Rigatelli, G. Zuliani, Diabetic patients with COVID-19 infection are at higher risk of ICU admission and poor short-term outcome, J. Clin. Virol. 127 (2020) 104354.

[13] X. Yang, Y. Yu, J. Xu, H. Shu, J. Xia, H. Liu, Y. Wu, L. Zhang, Z. Yu, M. Fang, T. Yu, Y. Wang, S. Pan, X. Zou, S. Yuan, Y. Shang, Clinical course and outcomes of critically ill patients with SARS-CoV-2 pneumonia in Wuhan, China: a single-centered, retrospective, observational study, Lancet Respir. Med. 8 (2020) 475–481.

[14] A. Remuzzi, G. Remuzzi, COVID-19 and Italy: what next? Lancet 395 (2020) 1225–1228.

[15] C. Lazzari, A. Shoka, A. Nusair, M. Rabottini, Psychiatry in time of COVID-19 pandemic, Psychiatr. Danub. 32 (2) (2020) 229–235.

[16] AS Yasin, Prevalence, Intensity and Manifestation of COVID-19 Fear: A Cross Sectional Analysis, Psychiatr. Danub. 32 (3–4) (2020) 499–504.

[17] R.P. Rajkumar, Attachment theory and psychological responses to the COVID-19 pandemic: a narrative review, Psychiatr. Danub. 32 (2) (2020) 256–261.

[18] B. Shi, H. Ye, A.A. Heidari, L. Zheng, Z. Hu, H. Chen, H. Turabieh, M. Mafarja, P. Wu, Analysis of COVID-19 severity from the perspective of coagulation index using evolutionary machine learning with enhanced brain storm optimization, Journal of King Saud University - Computer and Information Sciences (2021) 1319–1578, https://doi.org/10.1016/j.jksuci.2021.09.019.

[19] B. Shi, H. Ye, J. Zheng, Y. Zhu, A.A. Heidari, L. Zheng, H. Chen, L. Wang, P. Wu, Early recognition and discrimination of COVID-19 severity using slime mould support vector machine for medical decision-making, IEEE Access 9 (2021) 121996–122015.

[20] B. Shi, H. Ye, L. Zheng, J. Lyu, C. Chen, A.A. Heidari, Z. Hu, H. Chen, P. Wu, Evolutionary warning system for COVID-19 severity: colony predation algorithm enhanced extreme learning machine, Comput. Biol. Med. 136 (2021) 104698.

[21] H. Ye, P. Wu, T. Zhu, Z. Xiao, X. Zhang, L. Zheng, R. Zheng, Y. Sun, W. Zhou, Q. Fu, X. Ye, A. Chen, S. Zheng, A.A. Heidari, M. Wang, J. Zhu, H. Chen, J. Li, Diagnosing coronavirus disease 2019 (COVID-19): efficient Harris hawks-inspired fuzzy K-nearest neighbor prediction methods, IEEE Access 9 (2021) 17787–17802.

[22] Q. Zhang, Z. Wang, A.A. Heidari, W. Gui, Q. Shao, H. Chen, A. Zaguia, H. Turabieh, M. Chen, Gaussian Barebone salp swarm algorithm with stochastic fractal search for medical image segmentation: a COVID-19 case study, Comput. Biol. Med. (2021) 104941.

[23] L. Liu, D. Zhao, F. Yu, A.A. Heidari, C. Li, J. Ouyang, H. Chen, M. Mafarja, H. Turabieh, J. Pan, Ant colony optimization with Cauchy and greedy Levy mutations for multilevel COVID 19 X-ray image segmentation, Comput. Biol. Med. 136 (2021) 104609.

[24] T.D. Pham, Classification of COVID-19 chest X-rays with deep learning: new models or fine tuning? Health Inf. Sci. Syst. 9 (2021).

[25] M. Canayaz, MH-COVIDNet, Diagnosis of COVID-19 using deep neural networks and meta-heuristic-based feature selection on X-ray images, Biomed. Signal Process Control 64 (2021), 102257-102257.

[26] R.A. Al-Falluji, Z.D. Katheeth, B. Alathari, Automatic detection of COVID-19 using chest X-ray images and modified ResNet18-based convolution neural networks, Cmc-Computers Materials & Continua 66 (2021) 1301–1313.

[27] W.M. Shaban, A.H. Rabie, A.I. Saleh, M.A. Abo-Elsoud, Detecting COVID-19 Patients Based on Fuzzy Inference Engine and Deep Neural Network, Applied soft computing, 2020, 106906-106906.

[28] L. Sun, Z. Mo, F. Yan, L. Xia, F. Shan, Z. Ding, B. Song, W. Gao, W. Shao, F. Shi, H. Yuan, H. Jiang, D. Wu, Y. Wei, Y. Gao, H. Sui, D. Zhang, D. Shen, Adaptive feature selection guided deep forest for COVID-19 classification with chest CT, Ieee Journal of Biomedical and Health Informatics 24 (2020) 2798–2805.

[29] W.M. Shaban, A.H. Rabie, A.I. Saleh, M.A. Abo-Elsoud, A New COVID-19 Patients Detection Strategy (CPDS) Based on Hybrid Feature Selection and Enhanced KNN Classifier, Knowledge-Based Systems, 2020, p. 205.

[30] L. Dey, S. Chakraborty, A. Mukhopadhyay, Machine learning techniques for sequence-based prediction of viral-host interactions between SARS-CoV-2 and human proteins, Biomed. J. 43 (2020) 438–450.

[31] B. Abraham, M.S. Nair, Computer-aided detection of COVID-19 from X-ray images using multi-CNN and Bayesnet classifier, Biocybernetics and biomedical engineering 40 (2020) 1436–1445.

[32] C. Liu, X. Wang, C. Liu, Q. Sun, W. Peng, Differentiating novel coronavirus pneumonia from general pneumonia based on machine learning, Biomed. Eng. Online 19 (2020).

[33] T. Tuncer, S. Dogan, F. Ozyurt, An automated Residual Exemplar Local Binary Pattern and iterative ReliefF based COVID-19 detection method using chest X-ray image, Chemometr. Intell. Lab. Syst. 203 (2020) 11.

[34] E. Casiraghi, D. Malchiodi, G. Trucco, M. Frasca, L. Cappelletti, T. Fontana, A. A. Esposito, E. Avola, A. Jachetti, J. Reese, A. Rizzi, P.N. Robinson, G. Valentini, Explainable machine learning for early assessment of COVID-19 risk prediction in emergency departments, Ieee Access 8 (2020) 196299–196325.

[35] D.C.R. Novitasari, R. Hendradi, R.E. Caraka, Y. Rachmawati, N.Z. Fanani, A. Syarifudin, T. Toharudin, R.C. Chen, Detection OF COVID-19 chest X-ray using support vector machine and convolutional neural network, Communications in Mathematical Biology and Neuroscience (2020) 2052–2541.

[36] P. Wu, H. Ye, X. Cai, C. Li, S. Li, M. Chen, M. Wang, A.A. Heidari, M. Chen, J. Li, An effective machine learning approach for identifying non-severe and severe coronavirus disease 2019 patients in a rural Chinese population: the wenzhou retrospective study, IEEE Access 9 (2021) 45486–45503.

[37] A.A. Heidari, S. Mirjalili, H. Faris, I. Aljarah, M. Mafarja, H. Chen, Harris hawks optimization: algorithm and applications, Future Generation Computer Systems-the International Journal of Escience 97 (2019) 849–872.

[38] T. Wang, W. Liu, J. Zhao, X. Guo, V. Terzija, A rough set-based bio-inspired fault diagnosis method for electrical substations, Int. J. Electr. Power Energy Syst. 119 (2020) 105961, https://doi.org/10.1016/j.ijepes.2020.105961.

[39] H. Moayedi, A. Mosavi, Synthesizing multi-layer perceptron network with ant lion biogeography-based dragonfly algorithm evolutionary strategy invasive weed and league champion optimization hybrid algorithms in predicting heating load in residential buildings, Sustainability 13 (2021) 3198.

[40] H. Moayedi, A. Mosavi, Suggesting a stochastic fractal search paradigm in combination with artificial neural network for early prediction of cooling load in residential buildings, Energies 14 (2021) 1649.

[41] H. Moayedi, A. Mosavi, An innovative metaheuristic strategy for solar energy management through a neural networks framework, Energies 14 (2021) 1196.

[42] H. Moayedi, A. Mosavi, Electrical power prediction through a combination of multilayer perceptron with water cycle ant lion and satin bowerbird searching optimizers, Sustainability 13 (2021) 2336.

[43] J. Tu, H. Chen, M. Wang, A.H. Gandomi, The colony predation algorithm, JBE 18 (2021) 674–710.

[44] H. Chen, S. Jiao, M. Wang, A.A. Heidari, X. Zhao, Parameters identification of photovoltaic cells and modules using diversification-enriched Harris hawks optimization with chaotic drifts, J. Clean. Prod. 244 (2020) 118778.

[45] H.M. Ridha, A.A. Heidari, M. Wang, H. Chen, Boosted mutation-based Harris hawks optimizer for parameters identification of single-diode solar cell models, Energy Convers. Manag. 209 (2020) 112660.

[46] S. Jiao, G. Chong, C. Huang, H. Hu, M. Wang, A.A. Heidari, H. Chen, X. Zhao, Orthogonally adapted Harris hawks optimization for parameter estimation of photovoltaic models, Energy 203 (2020) 117804.

[47] Y. Liu, G. Chong, A.A. Heidari, H. Chen, G. Liang, X. Ye, Z. Cai, M. Wang, Horizontal and vertical crossover of Harris hawk optimizer with Nelder-Mead simplex for parameter estimation of photovoltaic models, Energy Convers. Manag. 223 (2020) 113211.

[48] Y. Zhang, R. Liu, X. Wang, H. Chen, C. Li, Boosted binary Harris hawks optimizer and feature selection, Eng. Comput. 37 (2021) 3741–3770.

[49] J. Too, G. Liang, H. Chen, Memory-based Harris Hawk Optimization with Learning Agents: a Feature Selection Approach, Engineering with Computers, 2021.

[50] Y. Wei, H. Lv, M. Chen, M. Wang, A.A. Heidari, H. Chen, C. Li, Predicting entrepreneurial intention of students: an extreme learning machine with Gaussian barebone Harris hawks optimizer, IEEE Access 8 (2020) 76841–76855.

[51] H. Chen, A.A. Heidari, H. Chen, M. Wang, Z. Pan, A.H. Gandomi, Multi-population differential evolution-assisted Harris hawks optimization: framework and case studies, Future Generat. Comput. Syst. 111 (2020) 175–198.

[52] M.A. Al-Betar, M.A. Awadallah, A.A. Heidari, H. Chen, H. Al-khraisat, C. Li, Survival exploration strategies for Harris hawks optimizer, Expert Syst. Appl. 168 (2021) 114243.

[53] C. Li, J. Li, H. Chen, M. Jin, H. Ren, Enhanced Harris hawks optimization with multi-strategy for global optimization tasks, Expert Syst. Appl. 185 (2021) 115499.

[54] P. Jangir, A.A. Heidari, H. Chen, Elitist non-dominated sorting Harris hawks optimization: framework and developments for multi-objective problems, Expert Syst. Appl. 186 (2021) 115747.

[55] Z. Cai, J. Gu, J. Luo, Q. Zhang, H. Chen, Z. Pan, Y. Li, C. Li, Evolving an optimal kernel extreme learning machine by using an enhanced grey wolf optimization strategy, Expert Syst. Appl. 138 (2019) 112814.

[56] H. Chen, Q. Zhang, J. Luo, Y. Xu, X. Zhang, An enhanced Bacterial Foraging Optimization and its application for training kernel extreme learning machine, Appl. Soft Comput. 86 (2020) 105884.

[57] J. Luo, H. Chen, Z. Hu, H. Huang, P. Wang, X. Wang, X. Lv, C. Wen, A new kernel extreme learning machine framework for somatization disorder diagnosis, IEEE Access 7 (2019) 45512–45525.

[58] X. Wang, Z. Wang, J. Weng, C. Wen, H. Chen, X. Wang, A new effective machine learning framework for sepsis diagnosis, IEEE Access 6 (2018) 48300–48310.

[59] M. Wang, H. Chen, B. Yang, X. Zhao, L. Hu, Z. Cai, H. Huang, C. Tong, Toward an optimal kernel extreme learning machine using a chaotic moth-flame optimization strategy with applications in medical diagnoses, Neurocomputing 267 (2017) 69–84.

[60] Q. Li, H. Chen, H. Huang, X. Zhao, Z. Cai, C. Tong, W. Liu, X. Tian, An enhanced grey wolf optimization based feature selection wrapped kernel extreme learning machine for medical diagnosis, Computational and mathematical methods in medicine (2017) 2017.

[61] H.-L. Chen, G. Wang, C. Ma, Z.-N. Cai, W.-B. Liu, S.-J. Wang, An efficient hybrid kernel extreme learning machine approach for early diagnosis of Parkinson's disease, Neurocomputing 184 (2016) 131–144.

[62] J. Luo, H. Chen, Q. zhang, Y. Xu, H. Huang, X. Zhao, An improved grasshopper optimization algorithm with application to financial stress prediction, Appl. Math. Model. 64 (2018) 654–668.

[63] D. Zhao, C. Huang, Y. Wei, F. Yu, M. Wang, H. Chen, An effective computational model for bankruptcy prediction using kernel extreme learning machine approach, Comput. Econ. 49 (2017) 325–341.

[64] X. Zhao, D. Li, B. Yang, S. Liu, Z. Pan, H. Chen, An efficient and effective automatic recognition system for online recognition of foreign fibers in cotton, IEEE Access 4 (2016) 8465–8475.

[65] T. Wang, X. Wei, J. Wang, T. Huang, H. Peng, X. Song, M.J. Perez-Jimenez, A weighted corrective fuzzy reasoning spiking neural P system for fault diagnosis in power systems with variable topologies, Eng. Appl. Artif. Intell. 92 (2020) 103680.

[66] S. Mirjalili, Moth-flame optimization algorithm: a novel nature-inspired heuristic paradigm, Knowl. Base Syst. 89 (2015) 228–249.

[67] S. Mirjalili, A. Lewis, The whale optimization algorithm, Adv. Eng. Software 95 (2016) 51–67.

[68] S. Mirjalili, S.M. Mirjalili, A. Lewis, Grey wolf optimizer, Adv. Eng. Software 69 (2014) 46–61.

[69] G.-B. Huang, H. Zhou, X. Ding, R. Zhang, Extreme learning machine for regression and multiclass classification, IEEE Trans. Syst. Man Cybern. B Cybern. 42 (2012) 513–529.

[70] H. Chen, S. Li, A.A. Heidari, P. Wang, J. Li, Y. Yang, M. Wang, C. Huang, Efficient multi-population outpost fruit fly-driven optimizers: framework and advances in support vector machines, Expert Syst. Appl. 142 (2020) 112999.

[71] J. Hu, Y. Liu, A.A. Heidari, Y. Bano, A. Ibrohimov, G. Liang, H. Chen, X. Chen, A. Zaguia, H. Turabieh, An effective model for predicting serum albumin levels in hemodialysis patients, Comput. Biol. Med. (2021) 105054.

[72] G.B. Huang, H. Zhou, X. Ding, R. Zhang, Extreme learning machine for regression and multiclass classification, IEEE Trans. Syst. Man Cybern. B Cybern. 42 (2012) 513–529.

[73] J. Hu, W. Gui, A.A. Heidari, Z. Cai, G. Liang, H. Chen, Z. Pan, Dispersed foraging slime mould algorithm: continuous and binary variants for global optimization and wrapper-based feature selection, Knowl. Base Syst. 237 (2022) 107761.

[74] J. Hu, A.A. Heidari, L. Zhang, X. Xue, W. Gui, H. Chen, Z. Pan, Chaotic diffusion-limited aggregation enhanced grey wolf optimizer: insights, analysis, binarization, and feature selection, Int. J. Intell. Syst. (2022) 0884–8173.

[75] J. Hu, Y. Liu, A.A. Heidari, Y. Bano, A. Ibrohimov, G. Liang, H. Chen, X. Chen, A. Zaguia, H. Turabieh, An effective model for predicting serum albumin level in hemodialysis patients, Comput. Biol. Med. 140 (2022) 105054.

[76] Y. Xu, H. Huang, A.A. Heidari, W. Gui, X. Ye, Y. Chen, H. Chen, Z. Pan, MFeature: towards high performance evolutionary tools for feature selection, Expert Syst. Appl. 186 (2021) 115655.

[77] S. Wu, P. Mao, R. Li, Z. Cai, A.A. Heidari, J. Xia, H. Chen, M. Mafarja, H. Turabieh, X. Chen, Evolving fuzzy k-nearest neighbors using an enhanced sine cosine algorithm: case study of lupus nephritis, Comput. Biol. Med. 135 (2021) 104582.

[78] J. Hu, H. Chen, A.A. Heidari, M. Wang, X. Zhang, Y. Chen, Z. Pan, Orthogonal learning covariance matrix for defects of grey wolf optimizer: insights, balance, diversity, and feature selection, Knowl. Base Syst. 213 (2021) 106684.

[79] X. Zhang, R. Jiang, T. Wang, J. Wang, Recursive neural network for video deblurring, IEEE Trans. Circ. Syst. Video Technol. 31 (2021) 3025–3036.

[80] X.Y. Cao, J.X. Wang, J.H. Wang, B. Zeng, A risk-averse conic model for networked microgrids planning with reconfiguration and reorganizations, IEEE Trans. Smart Grid 11 (2020) 696–709.

[81] Z. Wu, R. Li, J. Xie, Z. Zhou, J. Guo, X. Xu, A user sensitive subject protection approach for book search service, Journal of the Association for Information Science and Technology 71 (2020) 183–195.

[82] Z. Wu, S. Shen, X. Lian, X. Su, E. Chen, A dummy-based user privacy protection approach for text information retrieval, Knowl. Base Syst. 195 (2020) 105679.

[83] Z. Wu, S. Shen, H. Zhou, H. Li, C. Lu, D. Zou, An effective approach for the protection of user commodity viewing privacy in e-commerce website, Knowl. Base Syst. 220 (2021) 106952.

[84] X. Zhang, T. Wang, J. Wang, G. Tang, L. Zhao, Pyramid channel-based feature attention network for image dehazing, Comput. Vis. Image Understand. (2020) 197–198, 103003.

[85] Z. Zhang, L. Wang, W. Zheng, L. Yin, R. Hu, B. Yang, Endoscope image mosaic based on pyramid ORB, Biomed. Signal Process Control 71 (2022) 103261.

[86] S. Qiu, Z. Hao, Z. Wang, L. Liu, J. Liu, H. Zhao, G. Fortino, Sensor Combination Selection Strategy for Kayak Cycle Phase Segmentation Based on Body Sensor Networks, IEEE Internet of Things Journal, 2021, https://doi.org/10.1109/JIOT.2021.3102856.

[87] S. Qiu, H. Zhao, N. Jiang, D. Wu, G. Song, H. Zhao, Z. Wang, Sensor network oriented human motion capture via wearable intelligent system, Int. J. Intell. Syst. (2021) 0884–8173, https://doi.org/10.1002/int.22689.

[88] H. Cui, Y. Guan, H. Chen, W. Deng, A novel advancing signal processing method based on coupled multi-stable stochastic resonance for fault detection, Appl. Sci. 11 (2021) 5385.

[89] Z. Zhang, P. Ma, R. Ahmed, J. Wang, D. Akin, F. Soto, U. Demirci, Advanced Point-of-Care Testing Technologies for Human Acute Respiratory Virus Detection, Adv. Mater. 2103646 (2021), https://doi.org/10.1002/adma.202103646.

[90] Y. Zhou, G. Xu, K. Tang, L. Tian, Y. Sun, Video coding optimization in AVS2, Inf. Process. Manag. 59 (2022) 102808.

[91] H. Liu, X. Xu, E. Li, S. Zhang, X. Li, Anomaly detection with representative neighbors, IEEE Transact. Neural Networks Learn. Syst. (2021) 1–11.

[92] Z. Wu, G. Li, S. Shen, Z. Cui, X. Lian, G. Xu, Constructing dummy query sequences to protect location privacy and query privacy in location-based services, World Wide Web 24 (2021) 25–49.

[93] Z. Wu, R. Wang, Q. Li, X. Lian, G. Xu, A location privacy-preserving system based on query range cover-up for location-based services, IEEE Trans. Veh. Technol. (2020) 69.

[94] H. Liu, X. Li, S. Zhang, Q. Tian, Adaptive hashing with sparse matrix factorization, IEEE Transact. Neural Networks Learn. Syst. 31 (2020) 4318–4329.

[95] M. Wang, Q. Zhang, H. Chen, A.A. Heidari, M. Mafarja, H. Turabieh, Evaluation of constraint in photovoltaic cells using ensemble multi-strategy shuffled frog leading algorithms, Energy Convers. Manag. 244 (2021) 114484.

[96] W. Deng, X. Zhang, Y. Zhou, Y. Liu, W. Deng, H. Chen, H. Zhao, An Enhanced Fast Non-dominated Solution Sorting Genetic Algorithm for Multi-Objective Problems, Information Sciences, 2021, https://doi.org/10.1016/j.ins.2021.1011.1052.

[97] K.W. Choi, T.N. Chau, O. Tsang, E. Tso, M.C. Chiu, W.L. Tong, P.O. Lee, T.K. Ng, W.F. Ng, K.C. Lee, W. Lam, W.C. Yu, J.Y. Lai, S.T. Lai, Outcomes and prognostic factors in 267 patients with severe acute respiratory syndrome in Hong Kong, Ann. Intern. Med. 139 (2003) 715–723.

[98] K.H. Hong, J.P. Choi, S.H. Hong, J. Lee, J.S. Kwon, S.M. Kim, S.Y. Park, J.Y. Rhee, B.N. Kim, H.J. Choi, E.C. Shin, H. Pai, S.H. Park, S.H. Kim, Predictors of mortality in Middle East respiratory syndrome (MERS), Thorax 73 (2018) 286–289.

[99] S.L. Smits, A. de Lang, J.M. van den Brand, L.M. Leijten, I.W.F. van, M. J. Eijkemans, G. van Amerongen, T. Kuiken, A.C. Andeweg, A.D. Osterhaus, B. L. Haagmans, Exacerbated innate host response to SARS-CoV in aged non-human primates, PLoS Pathog. 6 (2010), e1000756.

[100] F. Zhou, T. Yu, R. Du, G. Fan, Y. Liu, Z. Liu, J. Xiang, Y. Wang, B. Song, X. Gu, L. Guan, Y. Wei, H. Li, X. Wu, J. Xu, S. Tu, Y. Zhang, H. Chen, B. Cao, Clinical course and risk factors for mortality of adult inpatients with COVID-19 in Wuhan, China: a retrospective cohort study, Lancet 395 (2020) 1054–1062.

[101] T. Yu, S. Cai, Z. Zheng, X. Cai, Y. Liu, S. Yin, J. Peng, X. Xu, Association between clinical manifestations and prognosis in patients with COVID-19, Clin. Therapeut. 42 (2020) 964–972.

[102] S.M. Opal, T.D. Girard, E.W. Ely, The immunopathogenesis of sepsis in elderly patients, Clin. Infect. Dis. 41 (Suppl 7) (2005) S504–S512.

[103] J.A. Collins, A. Rudenski, J. Gibson, L. Howard, R. O'Driscoll, Relating oxygen partial pressure, saturation and content: the haemoglobin-oxygen dissociation curve, Breathe 11 (2015) 194–201.

[104] J. Xie, N. Covassin, Z. Fan, P. Singh, W. Gao, G. Li, T. Kara, V.K. Somers, Association between hypoxemia and mortality in patients with COVID-19, Mayo Clin. Proc. 95 (2020) 1138–1147.

[105] R. Zhang, Y. Wu, M. Zhao, C. Liu, L. Zhou, S. Shen, S. Liao, K. Yang, Q. Li, H. Wan, Role of HIF-1alpha in the regulation ACE and ACE2 expression in hypoxic human pulmonary artery smooth muscle cells, Am. J. Physiol. Lung Cell Mol. Physiol. 297 (2009) L631–L640.

[106] N. Shved, G. Warsow, F. Eichinger, D. Hoogewijs, S. Brandt, P. Wild, M. Kretzler, C.D. Cohen, M.T. Lindenmeyer, Transcriptome-based network analysis reveals

renal cell type-specific dysregulation of hypoxia-associated transcripts, Sci. Rep. 7 (2017) 8576.
[107] D. Wrapp, N. Wang, K.S. Corbett, J.A. Goldsmith, C.L. Hsieh, O. Abiona, B. S. Graham, J.S. McLellan, Cryo-EM structure of the 2019-nCoV spike in the prefusion conformation, Science 367 (2020) 1260–1263.
[108] Z. Varga, A.J. Flammer, P. Steiger, M. Haberecker, R. Andermatt, A. S. Zinkernagel, M.R. Mehra, R.A. Schuepbach, F. Ruschitzka, H. Moch, Endothelial cell infection and endotheliitis in COVID-19, Lancet 395 (2020) 1417–1418.
[109] L. Spiezia, A. Boscolo, F. Poletto, L. Cerruti, I. Tiberio, E. Campello, P. Navalesi, P. Simioni, COVID-19-Related severe hypercoagulability in patients admitted to intensive care unit for acute respiratory failure, Thromb. Haemostasis 120 (2020) 998–1000.
[110] N. Shenoy, R. Luchtel, P. Gulani, Considerations for target oxygen saturation in COVID-19 patients: are we under-shooting? BMC Med. 18 (2020) 260.
[111] J.L. Seifter, Integration of acid-base and electrolyte disorders, N. Engl. J. Med. 371 (2014) 1821–1831.
[112] W.J. Guan, Z.Y. Ni, Y. Hu, W.H. Liang, C.Q. Ou, J.X. He, L. Liu, H. Shan, C.L. Lei, D.S.C. Hui, B. Du, L.J. Li, G. Zeng, K.Y. Yuen, R.C. Chen, C.L. Tang, T. Wang, P. Y. Chen, J. Xiang, S.Y. Li, J.L. Wang, Z.J. Liang, Y.X. Peng, L. Wei, Y. Liu, Y.H. Hu, P. Peng, J.M. Wang, J.Y. Liu, Z. Chen, G. Li, Z.J. Zheng, S.Q. Qiu, J. Luo, C.J. Ye, S.Y. Zhu, N.S. Zhong, Clinical characteristics of coronavirus disease 2019 in China, N. Engl. J. Med. 382 (2020) 1708–1720.
[113] G.Q. Qian, N.B. Yang, F. Ding, A.H.Y. Ma, Z.Y. Wang, Y.F. Shen, C.W. Shi, X. Lian, J.G. Chu, L. Chen, Z.Y. Wang, D.W. Ren, G.X. Li, X.Q. Chen, H.J. Shen, X.M. Chen, Epidemiologic and clinical characteristics of 91 hospitalized patients with COVID-19 in Zhejiang, China: a retrospective, multi-centre case series, QJM 113 (2020) 474–481.
[114] G. Hernandez, R. Bellomo, J. Bakker, The ten pitfalls of lactate clearance in sepsis, Intensive Care Med. 45 (2019) 82–85.
[115] A. Bahl, M.N. Van Baalen, L. Ortiz, N.W. Chen, C. Todd, M. Milad, A. Yang, J. Tang, M. Nygren, L. Qu, Early predictors of in-hospital mortality in patients with COVID-19 in a large American cohort, Intern Emerg Med 15 (2020) 1485–1499.
[116] O.J. McElvaney, N.L. McEvoy, O.F. McElvaney, T.P. Carroll, M.P. Murphy, D. M. Dunlea, N.C. O, J. Clarke, E. O'Connor, G. Hogan, D. Ryan, I. Sulaiman, C. Gunaratnam, P. Branagan, M.E. O'Brien, R.K. Morgan, R.W. Costello, K. Hurley, S. Walsh, E. de Barra, C. McNally, S. McConkey, F. Boland, S. Galvin, F. Kiernan, J. O'Rourke, R. Dwyer, M. Power, P. Geoghegan, C. Larkin, R. A. O'Leary, J. Freeman, A. Gaffney, B. Marsh, G.F. Curley, N.G. McElvaney, Characterization of the inflammatory response to severe COVID-19 illness, Am. J. Respir. Crit. Care Med. 202 (2020) 812–821.